Fused deposition modeling (FDM) based 3D printing of microelectrodes and multi-electrode probes

Mariela Alicia Brites Helú, Liang Liu

Fused Deposition Modeling (FDM) based 3D printing of microelectrodes and multi-electrode probes

*Mariela Alicia Brites Helú and Liang Liu**

Université de Lorraine, CNRS, Laboratoire de Chimie Physique et Microbiologie pour les Matériaux et l'Environnement (LCPME), F-54000 Nancy, France

**Email: liang.liu@univ-lorraine.fr*

Abstract

Electrode fabrication is one of the basic practices for electrochemists. Especially, microelectrodes are generally known as "hand-made" and their fabrication is often like an art. In this work, we report a new protocol for fabricating microelectrodes and multi-electrode probes based on recently matured 3D Fused Deposition Modeling (FDM) printing technique. The general concept is to print half of the insulating body in PETG, insert the (etched) metal or carbon wire(s) in the channel(s), and resume printing to complete the whole electrode. The printed electrodes are then sealed by heating and mechanically polished before use. The process requires only low-cost non-specialized facilities that can be easily equipped even in teaching laboratories. Single microelectrodes of Pt, C, Au, Ag, W and Cu with diameter below 5 µm are fabricated and examined by cyclic voltammetry and scanning electron microscopy. Furthermore, a multi-electrode probe consisting of W, Cu, Ag (oxidized to Ag/AgCl) and Pt is also printed and demonstrated for pH (potentiometric) and H_2O_2 (amperometric) sensing applications.

Keywords: 3D printing, fused deposition modeling, microelectrode fabrication, multi-electrode probe for electroanalysis

1. Introduction

Over the last decades, 3D printing technologies have been well established in numerous application fields from aircraft, construction to chemical science and medical care[1–4]. In particular, Fused Deposition Modeling (FDM) has a tremendous impact not only for rapid prototyping and pre-production but also for mid-scale manufacturing of end-use products. FDM 3D printers build 3-dimensional objects adding layer by layer of thermoplastic materials which are extruded through a heated nozzle with a micrometric opening. These materials can be functionalized in order to give specific properties to the final product such as hardness, conductivity, *etc*[5]. Nowadays, the price of FDM 3D printers has lowered to hundred-euro scale so that they become popular in non-specialized laboratories, educational institutions and even households.

Electrochemists have also benefited from this technological development. Apart from printing electrode holders which is becoming common practice in electrochemistry laboratories, FDM can also be used for printing electrodes and integral electrochemical devices[6–10]. In these approaches, the electrodes are typically made of conductive filaments that are based on mixing conductive nanomaterials in polymers such as poly-lactic acid (PLA) or acrylonitrile butadiene styrene (ABS)[11]. To achieve sufficiently high conductivity for electrochemical measurements, it requires high content of conductive materials in the thermoplastic polymeric matrix, which is not yet matured in materials engineering[12]. So far, only a few conductive filaments based on graphene or carbon nanotubes are available in the market. Besides, due to the limited lateral resolution, FDM printing can only yield macroelectrodes of hundreds of micron diameter.

Meanwhile, in electrochemistry, microelectrodes are of high interest due to low time constant and hemispherical diffusion. They are ideal for kinetic studies of rapid homogeneous or heterogeneous electrochemical reactions, electroanalysis of low detection limit and in small volume of solution, *etc*. They also constitute the basis for scanning electrochemical microscopy (SECM), where they are positioned close to samples for spatially localized electrochemical measurements. The traditional method of fabricating microelectrodes is based on sealing metal wires or carbon fibers in glass capillaries. The wires or fibers can either be pulled together with glass capillaries or inserted into pulled capillaries. The sealing is then carried out by melting the glass. In case the electrode material cannot sustain high temperature, epoxy resin is also used for sealing the gap between the electrode and the glass capillary. As most of the microelectrodes are handmade, over the years researchers have been constantly seeking easier methods for the fabrication. For example, Mauzeroll's group has reported an approach for making microelectrodes based on glass sealing in less than one hour[13]. Girault *et al.* have used polyethylene terephthalate (PET) channels made by microfabrication to suck carbon ink for fabricating soft SECM probes[14]. The electrodes can be bent during SECM scanning and can be regenerated by cutting when needed. Earlier attempt by Ramos *et al.* also used PTFE/FEP shrinking tubes to replace glass as shielding material, which lowered the sealing temperature down to 350 °C without compromising the chemical stability[15].

In this work, we report an alternative method for fabricating microelectrodes based on FDM 3D printing. The concept is to seal metal wires and/or carbon fibers in 3D printed insulating plastic shields. First, half of the insulating part of the electrode is printed, and the printing is paused. Then, metal wires and/or carbon fibers are horizontally placed in the channels, and the printing is resumed to cover them. At the end, the channels are

closed by melting the plastic at relatively low temperature (110 °C) to ensure good sealing. The electrodes are exposed by polishing and the diameter of the plastic shield can also be reduced by polishing with an angle if used for SECM. Polyethylene terephthalate-glycol (PETG) is used as the shield due to its high chemical resistance in aqueous and alcoholic media. The whole process requires only a commercial FDM printer, which is much cheaper than glass pullers and microfabrication instrumentation. It is highly versatile for different electrode materials (Cu, Pt, Au, W, Ag and C) due to the horizontal placement of the electrode wires (*e.g.* etched wires) and the low temperature epoxy-free sealing. Moreover, 3D printing offers high flexibility in the design of electrode geometry. Here, we demonstrate an example where multiple electrodes of different materials are accommodated in the same printed structure as integrated miniaturized electrochemical device for sensing pH and H_2O_2.

2. Experimental

2.1 Materials and chemicals

Clear Polyethylene Terephthalate-Glycol (PETG) filament of 1.75 mm diameter is purchased from Prusa (Prusa Research, Czech Republic). Metal wires of Cu (0.2 mm), W (0.3 mm) and Pt (0.025 mm, 0.1 mm), Au (0.025 mm) and Ag (0.050 mm, 0.1 mm) and C fibers (0.01 mm) are purchased from ChemPur (Germany).

Sodium phosphate (Na_3PO_4, 99%, Fluka), hexaammineruthenium(III) chloride ($Ru(NH_3)_6Cl_3$, 98%, Sigma), sulfuric acid (H_2SO_4, 98%, Sigma), hydrochloric acid (HCl, 37%, Sigma), sodium hydroxide (NaOH, Carlo-Erba), perchloric acid ($HClO_4$, 60%, Riedel de Haen), hydrogen peroxide (H_2O_2, 30%, Sigma), acetone (C_3H_6O, Sigma), phosphate buffer solution (PBS, pH= 7), borax/sodium hydroxide solutions (pH= 10, pH= 9, standard for pH calibration, Sigma), citric acid/sodium hydroxide/sodium chloride solution (pH= 4, standard for pH calibration, Sigma) are

used as received without further purification. All solutions are prepared using deionized water (R > 18.2 MΩ·cm). Commercial oral antiseptic solution is acquired from a local retail store.

2.2 Fabrication of 3D printed microelectrodes and multi-electrode probe

Metal wires are electrochemically etched to conical shape in a 2-electrode cell using a Pt-ring counter electrode on a DC/AC power supply (PeakTech, Germany). The setup is similar as that for fabricating scanning tunneling microscopy tips (**Figure 1**), and the detailed conditions are listed in **Table 1**[16–19]. For expensive or thin wires (such as Pt, Au, Ag and C fibers), the WE is made by a ~10 mm-long piece attached to a long Cu wire by silver epoxy. For low-cost materials (Cu and W), a long piece of wire is directly used as WE.

Table 1. Conditions employed in the electrochemical etching of metal wires and C fibers.

Material	Solution	Voltage	Time
Pt	1.5 mol/L $CaCl_2$ in 1:1 H_2O/Acetone (vol. ratio)	15 V AC	1 min
Au	HCl (conc.)	3 V DC	1 min
W	5 mol/L NaOH	17 V DC	50 s
Cu	0.5 mol/L H_2SO_4	3 V DC	2 min
Ag	MeOH/$HClO_4$ in 1:4 (vol. ratio)	3 V DC	30 s
C	5 mol/L NaOH	3.5 V DC	40 s

The general concept of the fabrication is to 3D print the insulating body of the microelectrodes or multi-electrode probe in two or multiple steps and embed etched metal or carbon wires in pre-designed channels during the pauses of the printing (**Figure 2**). The geometrical design is made based on the final shape of the electrode using Tinkercad (Autodesk, USA), a free web browser-based 3D modeling program. It

is exported in .stl format and then sliced and converted to .gcode using Prusa open source slicing software Slic3r (Prusa Research, Czech Republic). The .gcode files are then edited by NotePad++ to add commands that allow pausing and resuming the printing at a desired height. They are loaded to a Prusa i3 MMUS2 (Prusa Research, Czech Republic) FDM printer in single-filament mode using 0.25 mm E3D brass nozzle, and the only human intervention during the printing is inserting the etched electrode wires. After printing, the microelectrodes are sealed on a hot plate (covered by aluminum foil to prevent adhesion of melted plastic) at 110 ℃ for 2 min. This ensures a perfect sealing between PETG and the wires by deforming the polymer (glass transition temperature ~80 ℃) while not losing the shape of the design. Excess printed plastic is mechanically cut under an optical microscope, and then the electrode disc is exposed by standard polishing procedure on a microelectrode polisher (HEKA, Germany) up to 4000 grit. Note that the hardness of PETG is similar as that of glass (in Rockwell scale: glass *ca.* 80 and PETG *ca.* 85, exact values may vary depending on the manufacturer), thus no special precaution is needed as compared with polishing classical glass-shielded microelectrodes. Nevertheless, we strongly recommended to polish the electrodes under optical microscope taking advantage of the transparency of PETG. At the final stage, the microelectrodes are hand polished on a cloth with 0.3 μm alumina paste.

The design of single microelectrodes is illustrated in **Figure 3A.** The tip end has a dimension of 1 mm (width) × 1 mm (height). Several considerations have to be taken into account for the design. First, the size of the channels should adapt to the diameter of the electrode wires for a tight fit so they would not laterally move during the following steps of printing. In this work the width of the channels are designed equal to the diameter of the wires (0.2 mm for Cu and 0.3 mm for W). However, this value may need to be increased according to the tolerance of each printer/configuration which can

be easily determined by prior testing the fitting of a wire in different sized printed channels. Another consideration is the thickness of the insulating shield at the tip of the electrode. It is recommended to be at least two times the diameter of the nozzle for ensuring full coverage of the electrode wires (A failure example is shown in Supporting Information Figure S1). The most important trick is the "bridges" as shown in the cross-section view **(Figure 3B**). As the electrode wires are naturally bent from the spool, these "bridges" are essential for fixing the wires vertically so that they will not "jump" out of the channels during the printing. On the other hand, for the ease of inserting wires, it is recommended to limit the width of each "bridge" less than 1 mm and to have only three to four "bridges" for a channel of 5 cm long.

The pauses are set after the "bridges" are printed while before closing the channels. The layer height can be located in Slic3r software by visualizing the layers. In the .gcode file, pause/resume commands (detailed in Supporting Information) are added after this layer, so that the printer will stop with a beep notification and move the extruder away from the printing zone for the users to insert the wires. During the pause, the wires are horizontally inserted into the channels from the conical extreme of the shield and threaded like a strand through the bridges (Safety precaution: The extruder and the bed may still be hot so the operators should carefully avoid touching them!). Then the printing will resume after pressing the knob in the printer to fully cover the wires.

The selection of printing parameters mainly takes the default values for PETG in Slic3r software. The nozzle temperature is 250 ℃. The printing layer height is 0.05 mm (ultradetailed) and the printing speed is 30 mm/s. The bed temperature is increased to 100 ℃ for ensuring better adhesion between the printed structure and the heat bed. This is helpful for preventing lateral displacement during the insertion of electrode wires.

The percentage of filling is set 20%, which is sufficient to be rigid due to the small size of the printed microelectrodes.

Single microelectrodes of Cu, Pt, Au, W, Ag and C are printed using the above-mentioned protocol. As a further step, we also fabricated a multi-electrode probe consisting of four different materials (Cu, W, Ag and Pt) for demonstrating the electrochemical sensing applications. The probe is in rectangular shape with dimensions of 60 mm (length) × 4 mm (width) × 3 mm (thickness), holding four separate microchannels in a square of 1.4 mm by 1.4 mm (**Figure 3C and 3D**). The channels are designed wider at one extreme to insert jumper wire connectors of 0.6 mm diameter. The printing protocol is similar as that for single microelectrodes, except that two pauses are made for inserting the electrode wires at different layers (two in the first pause and two in the second). After polishing, the metal disc electrodes in the multi-electrode probe are further functionalized. Ag is oxidized at 0.5 V (*vs.* Ag wire) for 120 s in 1M HCl forming Ag/AgCl quasi reference electrode (QRE). Then the probe is aged in phosphate buffer solution for 12 h to achieve stable Cu and W surface for potentiometric and amperometric sensing measurements. The final diameter of the electrodes is 66 µm, 84 µm, 100 µm and 100 µm for Cu, W, Ag/AgCl and Pt, respectively.

For each microelectrode, the printing takes less than 5 min before inserting the wires and another 5 min for completing the designed structure. Up to 42 microelectrodes can be printed in one batch. The exact values may slightly differ according to the printer and the geometric design, but it is more efficient than most of the classical methods of microelectrode fabrication. The .stl and .gcode (with pause) files for single microelectrode and multi-electrode probes are shared in Supporting Information.

2.3 Characterizations of 3D printed microelectrodes and multi-electrode probe

2.3.1 Optical and scanning electron microscopy inspections

Optical inspection is carried out at different stages of the fabrication on an optical microscope (Nikon, Japan) coupled with digital camera (Bresser, Germany). It is also used for visually checking the quality of polished microelectrodes. Scanning electron microscopy (SEM) is performed on a JEOL JMS-IT500HR microscope (JEOL, Japan) with 3 kV acceleration voltage at current emission of 30 µA. Microelectrodes are coated with a 10 nm Au layer to prevent the charging on insulating PETG. They are vertically placed in the vacuum chamber with the tip facing up using a home-design 3D printed stub[20].

2.3.2 Electrochemical characterization by cyclic voltammetry

The electrochemical characterization of 3D printed microelectrodes is primarily based on cyclic voltammetry (CV) which is a recognized method for evaluating the electrode quality. The measurements are carried out on a PalmSens3 potentiostat (PalmSens, The Netherlands). A three-electrode system is used, where the 3D printed microelectrode acts as working electrode (WE), a Pt wire as counter-electrode (CE) and a commercial Ag/AgCl (in 1 mol/L KCl, from CHI, USA) as reference electrode (RE). The Pt, Au, C and Ag microelectrodes are cycled in 0.1 mol/L H_2SO_4. The Cu and W electrodes are measured in PBS (pH = 7.4). The scan rate is 0.1 V/s. All the microelectrodes are further characterized in 1mmol/L $Ru(NH_3)_6Cl_3$ + 0.1mol/L Na_3PO_4 at room temperature by scanning between 0 and –0.4 V at 0.05 V/s. All the solutions are deaerated by bubbling high purity N_2 for 10 min before electrochemical measurements.

2.4 Electrochemical sensing application examples of 3D printed multi-electrode probe

2.4.1 Potentiometric pH analysis

Taking advantage of the pH dependent open circuit potential of metallic tungsten electrodes[21], the 3D printed multi-electrode probe consisting of Cu, W, Ag/AgCl and Pt is used for potentiometric sensing of pH. Here, only two electrodes are connected, W as WE and Ag/AgCl as QRE/CE. The calibration curve (OCP *vs.* pH) is carried out in a series of standard buffer solutions of pH = 4, 7, 9 and 10. The OCP values are taken in a time period of 300 s. The pH measurements are performed in three different aqueous samples: tap water (S1), milli-Q water (S2) and commercial oral antiseptic solution (S3). The same solutions are also measured by a standard pH-meter (Radiometer, Denmark) as reference.

2.4.2 Amperometric determination of H_2O_2

The multi-electrode probe is also tested as amperometric sensor for H_2O_2. In this case, the 3D printed probe is connected as three-electrode system: Cu as WE, Ag/AgCl as QRE and Pt as CE. Current is recorded on Cu by applying –0.2 V *vs.* Ag/AgCl. Calibration curve is performed by consecutively adding different volumes of 20 mmol/L H_2O_2 solution in 0.1 mol/L phosphate buffer (pH = 7). After each addition, the solution is stirred for a few seconds to homogenize the concentration. For the determination of H_2O_2 in a commercial oral antiseptic solution (S3), 0.04 mL of S3 is added into 20 mL of phosphate buffer, and the steady-state current is measured in this diluted analyte. Quantification is achieved by standard addition method (*i.e.* further adding different volumes of 20 mmol/L H_2O_2 solution) to avoid interference from other components in the analyte[22].

3. Results and Discussion

3.1 Electrochemical behavior of 3D printed microelectrodes

The electrochemical behavior of 3D printed microelectrodes is studied by cyclic voltammetry (CV), which is a classical method for evaluating the quality of

electrodes[23]. First, the Pt, Au, Ag and C microelectrodes are cycled (30 scans) in 0.1 mol/L H_2SO_4, and the Cu and W microelectrodes are cycled (4 scans) in PBS buffer solution (pH = 7.4). The purpose is to obtain a predictable and clean electrode surface for subsequent measurements, as well as to verify the chemical quality of the electrodes. Then further electrochemical characterization is carried out in $Ru(NH_3)_6^{3+}$ redox media to evaluate the area and quality (sealing, geometry) of the exposed disc, which is in parallel supported by SEM images of the electrodes.

Figure 4 shows the second and last cycles voltammograms of 3D printed microelectrodes in 0.1 mol/L H_2SO_4 or PBS (pH = 7.4). The Pt microelectrode exhibits H absorption/desorption peaks at *ca.* –0.15 V (*vs.* Ag/AgCl), the absorption of O in the range of 0.6 to 1.0 V (*vs.* Ag/AgCl) and the sharp peak of reduction of platinum oxide at *ca.* 0.5 V (*vs.* Ag/AgCl, **Figure 4A**). The Au microelectrode voltammogram shows characteristic peaks of oxidation at *ca.* 1.0 V (*vs.* Ag/AgCl) and reduction at *ca.* 0.6 V (*vs.* Ag/AgCl, **Figure 4B**). The small differences between scans can be attributed to a re-structuration process of the surface gold oxides. The Ag microelectrode shows a well-defined redox couple at *ca*. 0.4 and 0.25 V (*vs.* Ag/AgCl) that is assigned to the formation and subsequent re-dissolution of Ag_2O[24,25]. Additional shoulders and small peaks at *ca.* 0.45 V (*vs.* Ag/AgCl) and peak at *ca.* 0.1 V (*vs.* Ag/AgCl) can be ascribed to various absorbed intermediates[24] (**Figure 4C**). The C microelectrode shows non-Faradaic behavior in the range of –0.3 to 0.9 V (*vs.* Ag/AgCl) and starts to oxidize when the potential is more positive than 0.9 V (*vs.* Ag/AgCl, **Figure 4D**). All these fit well the typical behavior that are extensively reported in literature. The Cu and W microelectrodes are measured in mild PBS (pH = 7.4) solution instead of strong acid for less cycles due to the ease of oxidation. Oxidation peaks can be seen for both metals, which reasonably indicate the good status of the electrodes[22,26,27].

Overall, the response of the 3D printed microelectrodes seems to be stable during cycling, not showing signs of contamination or filtration during the time of the experiments. Moreover, the 3D printed microelectrodes can be stored for at least two months without evident deterioration in their voltammetric response (Supporting Information, Figure S3). In the case of Ag, W and Cu, a thin oxide layer may form over time, but it can be removed simply by polishing with cloth which is anyway an essential step before using the electrodes.

Figure 5 depicts the redox behavior of 3D printed microelectrodes in deaerated 1mmol/L $Ru(NH_3)_6^{3+}$ solution. In all cases, the CV curves show well-defined sigmoidal shape that is stable over five scans. The charging current is relatively low, and there is no significant signal of infiltration of solution in the gap between the electrode disc and the PETG sealing. This classical evaluation indicates that the 3D printed microelectrodes are generally in good state, although sometimes we also observe poor sealing so that the electrodes must be discarded. From the diffusion-limited current (i_d), the radius of microelectrodes can be derived from the following equation:

$$i_d = 4nFDCa \quad \text{(Eq. 1)}$$

where n is the number of electron transferred, F is the Faraday constant, D and C are the diffusion coefficient and the bulk concentration of $Ru(NH_3)_6^{3+}$, and a is the radius of the microelectrode. The calculated radius is indicated in **Figure 5**, which fits well the radius observed by SEM except for C microelectrode. In the case of C microelectrode, it is seen from SEM image that the C disc is slightly above the PETG shield. This may explain the error and also shows the necessity of using SEM for the quality control of the microelectrodes[28]. Nevertheless, one has to be also careful not to expose the electrodes under electron beam for long time in SEM, as this may also damage the sealing due to the charging and heating of insulating PETG shield. Moreover, the

voltammograms of 3D printed microelectrodes in $Ru(NH_3)_6^{3+}$ are also stable after storage for two months (Supporting Information, Figure S4).

It should be noted that the quality of sealing is highly important for the fabrication of microelectrodes. As illustrated in **Figure 6A**, the as-printed structures present microscopic gaps between neighboring lines and layers even though they appear to be smooth. This is unacceptable for microelectrodes as they need to be used in solutions. One way to overcome this issue is over-extruding the filament resulting in overlapped printed lines with a better seal. However, this adds to inconsistency between the designed and printed dimension of the structure, thus it is also unfavored for high precision tasks. Here, we propose a heating post-treatment which practically seals the gaps. This is achieved by heating the 3D printed microelectrodes at 110 ℃ for 2 min. It partially softens and fuses the lines and layers as shown in **Figure 6B**. The concept is similar as melting glass for sealing microelectrodes in classical fabrication processes, yet it is carried out at much lower temperature. This offers several advantages: (1) it does not need vacuum line that prevents the oxidation of metal or carbon at high temperature; (2) it does not need precise control of slow heating and cooling for preventing the generation of gap between the electrode and the glass shield due to their different thermo-expansion coefficient; (3) it is applicable to electrode materials with melting point lower than capillary glass (~ 600 ℃). These advantages make the 3D printing-based protocol much more generic, as we demonstrate various materials in this work.

3.2 Multi-electrode probe as potentiometric pH sensor

Multi-electrode probes have been widely used in diverse fields such as physiology, electrocatalysis and scanning electrochemical probe techniques (scanning bipolar electrochemical microscopy[29], scanning electrochemical cell microscopy[30], local

electrochemical impedance spectroscopy[31], *etc.*). These probes are usually made by sealing multiple electrodes in theta or multi-barrel glass capillaries. 3D printing offers an alternative method for fabricating such multi-electrode probes. Due to limited resolution of printing, the distance between electrodes is difficult to reach the same order as pulled theta capillaries, yet it can be accurately controlled and customized in the range of hundreds of microns. This is sufficient for miniaturized sensing applications.

Over the years, solid-state pH sensors have been developed as complement to classical glass electrodes due to the high temperature applicability and mechanical stability. The most commonly used solid-state pH sensors are based on iridium oxides[32,33], but tungsten and tungsten oxides (WO_x) have also been reported to monitor pH based on open circuit potential measurements[21,34,35]. The tungsten redox equilibrium involves H^+ (Reaction 1), thus the equilibrium potential has pH dependence following Nernst Equation.

$$WO_x + 2yH^+ + 2ye^- \leftrightarrow WO_{x-y} + yH_2O \quad \text{(Reaction 1)}$$

The multi-electrode probe as shown in **Figure 3D** is used for pH sensing. The electrode is connected in two-electrode configuration, with W electrode (a = 42 μm) as WE and Ag/AgCl electrode (a = 50 μm) as RE/CE (Scheme in **Figure 7A**). The Pt and Cu electrodes are unconnected. **Figure 7B** shows the stable open circuit potential of the probe (W *vs.* Ag/AgCl QRE) in standard solutions of different pH. The potential is linear (R^2 = 0.9988) to pH in the range of 4 to 10, with a slope of –0.083 V/pH. After the four-point calibration, three aqueous samples (tap water (S1), milli-Q water (S2) and commercial oral antiseptic solution (S3)) are measured. From the potential, one may obtain pH from the calibration curve as shown with stars in **Figure 7B**. As comparison,

the same samples are measured with glass electrodes on a commercial pH meter, and the obtained values are quite close (S1: 7.7; S2: 8.5; S3: 6.2).

The results above indicate that the 3D printed multi-electrode probe could reliably serve as pH sensor for aqueous solutions. As compared with classical glass electrodes, the size of the probe is much smaller so that it can measure samples of small volume such as µL droplets. However, it should be noted that the time response of the probe is relatively slow (100 s). This is mainly due to the small size of both WE and RE, which makes the system more difficult to depolarize.

3.3 Multi-electrode probe as amperometric H_2O_2 sensor

The multi-electrode probe accommodates different electrodes that allow not only two-electrode potentiometric measurements but also more flexible measurements in three-electrode configuration. As copper electrodes have been reported for electroanalysis of glucose[36], nitrate[37] and H_2O_2[38] by amperometry, we demonstrate the amperometric analysis of H_2O_2 using the same 3D printed multi-electrode probe as shown in **Figure 3D**. A constant potential of –0.2 V is applied on the Cu electrode (a = 33 µm) versus the Ag/AgCl (a = 50 µm) QRE, and the Pt electrode (a = 50 µm) is connected as CE (**Figure 8A**). The W electrode is unconnected. **Figure 8B** shows the current variation while adding different volume of 20 mmol/L H_2O_2 aliquot into 5 mL of 0.1 mol/L PBS solution under stirring. After each addition, it is seen that the current reaches new stable value in *ca.* 10-30 s. This stable current (i_{ss}) originates from the electrochemical reduction of H_2O_2, and it is in linear relationship ($i_{ss}(\mu A) = -0.061 - 1.17C_{H_2O_2}(mmol/L)$, R^2 = 0.99942) with the concentration of H_2O_2 in the solution

(**Figure 8C**). This indicates that the 3D printed multi-electrode probe can be used for amperometric analysis of H_2O_2 in the range of 0 to 2 mmol/L.

Apart from pH as shown in **Figure 7**, the concentration of H_2O_2 in a commercial oral antiseptic solution (S3) is also analyzed by the 3D printed multi-electrode probe. Considering that the sample contains 0.5-3 % (0.16-0.98 mol/L) H_2O_2, it needs to be diluted to meet the linear range as shown in **Figure 8B**. Therefore, a 20 mL blank PBS solution is measured, and then 40 µL of S3 is added. This dilutes the sample and yields a significant increase in current due to the presence of H_2O_2, as shown in **Figure 9A**. From the steady current value and the calibration curve (**Figure 8B**), one may obtain the H_2O_2 concentration in diluted S3 to be 1.15 mmol/L. As the dilution factor is 500, the H_2O_2 concentration in the original sample S3 is 0.575 mol/L.

With the unknown species in S3 that might interfere the quantification, standard addition method is applied to eliminate this interference. Thus, different volume of 20 mmol/L H_2O_2 standard solution is added to the diluted S3 sample, and a new calibration curve is built by plotting the current increase as a function of H_2O_2 concentration increase (**Figure 9B**, $i_{ss}(\mu A) = -0.054 - 1.15C_{H_2O_2}(mmol/L)$, R^2 = 0.99982). The slope is almost the same as **Figure 8B**, indicating that the interference from unknown species is negligible. The concentration of S3b derived from the new calibration curve is 0.590 mol/L, which is also close to the value obtained from **Figure 8B**. The results further confirm the applicability of 3D printed multi-electrode probe for sensing applications, and multiple-task sensing (*e.g.* pH and H_2O_2) can be foreseen with the same probe.

4. Conclusions

We report a new protocol for fabricating microelectrodes and multi-electrode probes based on 3D FDM printing. The general concept is to print half of the insulating body in PETG, insert the (etched) metal or carbon wire(s) in the channel(s), and resume printing to complete the whole electrode. The wire(s) are sealed by heating at 110 ℃ for 2 min, and then they are exposed by mechanical polishing. Single microelectrodes of Pt, C, Au, Ag, W and Cu with diameter below 5 µm, and a multi-electrode probe consisting of W, Cu, Ag (oxidized to Ag/AgCl) and Pt are prepared by this method. The electrodes show good electrochemical performance and the sealing is verified by SEM. The multi-electrode probe is demonstrated for pH (potentiometric) and H_2O_2 (amperometric) sensing applications.

As compared with classical glass capillary-based fabrication of microelectrodes, the 3D printing-based process reduces the human intervention and may improve the production efficiency by printing up to 42 electrodes in a batch. The low temperature sealing also avoids oxidizing or melting the electrode, which broadens the applicable electrode materials. Besides, the whole process only requires an FDM printer, a hot plate, and an electrode polisher, which can be easily found or equipped even in teaching laboratories. The electrode geometry design and slicing are customizable and realized by free software. This paves the way for fabricating miniaturized electrochemical sensors as well as developing teaching experiments of microelectrodes. Future development may focus on reducing the diameter of the insulating shield of these 3D printed microelectrodes for scanning electrochemical probe applications.

Acknowledgements

The authors gratefully acknowledge financial support from CNRS MOMENTUM Project (2018-2020). The platform of Spectroscopies and Microscopies of Interfaces (SMI) of LCPME is also acknowledged for SEM characterizations.

References

[1] P. Wu, J. Wang, X. Wang, A critical review of the use of 3-D printing in the construction industry, Autom. Constr. 68 (2016) 21–31. https://doi.org/10.1016/j.autcon.2016.04.005.

[2] A.J. Capel, R.P. Rimington, M.P. Lewis, S.D.R. Christie, 3D printing for chemical, pharmaceutical and biological applications, Nat. Rev. Chem. 2 (2018) 422–436. https://doi.org/10.1038/s41570-018-0058-y.

[3] A. Awad, S.J. Trenfield, S. Gaisford, A.W. Basit, 3D printed medicines: A new branch of digital healthcare, Int. J. Pharm. 548 (2018) 586–596. https://doi.org/10.1016/j.ijpharm.2018.07.024.

[4] Y.W.D. Tay, B. Panda, S.C. Paul, N.A. Noor Mohamed, M.J. Tan, K.F. Leong, 3D printing trends in building and construction industry: a review, Virtual Phys. Prototyp. 12 (2017) 261–276. https://doi.org/10.1080/17452759.2017.1326724.

[5] S.C. Ligon, R. Liska, J. Stampfl, M. Gurr, R. Mülhaupt, Polymers for 3D Printing and Customized Additive Manufacturing, Chem. Rev. 117 (2017) 10212–10290. https://doi.org/10.1021/acs.chemrev.7b00074.

[6] F. Li, N.P. Macdonald, R.M. Guijt, M.C. Breadmore, Increasing the functionalities of 3D printed microchemical devices by single material, multimaterial, and print-pause-print 3D printing, Lab Chip. 19 (2019) 35–49. https://doi.org/10.1039/c8lc00826d.

[7] M. Cheng, R. Deivanayagam, R. Shahbazian- Yassar, 3D Printing of Electrochemical Energy Storage Devices: A Review of Printing Techniques and Electrode/Electrolyte Architectures, Batter. Supercaps. 3 (2020) 130–146.

https://doi.org/10.1002/batt.201900130.

[8] A. Ambrosi, M. Pumera, 3D-printing technologies for electrochemical applications, 2740 | Chem. Soc. Rev. 45 (2016) 2740–2755. https://doi.org/10.1039/c5cs00714c.

[9] V. Katseli, N. Thomaidis, A. Economou, C. Kokkinos, Miniature 3D-printed integrated electrochemical cell for trace voltammetric Hg(II) determination, Sensors Actuators B. 308 (2020) 127715–7. https://doi.org/10.1016/j.snb.2020.127715.

[10] N. Rohaizad, C.C. Mayorga-Martinez, F. Novotný, R.D. Webster, M. Pumera, 3D-printed Ag/AgCl pseudo-reference electrodes, Electrochem. Commun. 103 (2019) 104–108. https://doi.org/10.1016/j.elecom.2019.05.010.

[11] S.W. Kwok, K.H.H. Goh, Z.D. Tan, S.T.M. Tan, W.W. Tjiu, J.Y. Soh, Z.J.G. Ng, Y.Z. Chan, H.K. Hui, K.E.J. Goh, Electrically conductive filament for 3D-printed circuits and sensors, Appl. Mater. Today. 9 (2017) 167–175. https://doi.org/10.1016/j.apmt.2017.07.001.

[12] J.D. Horst, P.P. De Andrade Junior, C.A. Duvoisin, R. de A. Vieira, Fabrication of Conductive Filaments for 3D-printing: PolymerNanocomposites, BIOINTERFACE Res. Appl. Chem. 10 (2020) 6577–6586. https://doi.org/10.33263/BRIAC106.65776586.

[13] L. Danis, D. Polcari, A. Kwan, S.M. Gateman, J. Mauzeroll, Fabrication of Carbon, Gold, Platinum, Silver, and Mercury Ultramicroelectrodes with Controlled Geometry, Anal. Chem. 87 (2015) 2565–2569. https://doi.org/10.1021/ac503767n.

[14] F. Corté s-Salazar, M. Trä uble, F. Li, J.-M. Busnel, A.-L. Gassner, M. Hojeij, G. Wittstock, H.H. Girault, Soft Stylus Probes for Scanning Electrochemical Microscopy, Anal. Chem. 81 (2009) 6889–6896. https://doi.org/10.1021/ac900887u.

[15] B.L. Ramos, E.A. Blubaugh, T.H. Ridgway, W.R. Heineman, 7-Irradiation-Induced Grafting of Poly(styrenesulfonate) to Poly(tetrafluoroethylene) Shielded Microelectrodes, Biosens. Fundam. Appl. 66 (1994) 7–13. https://doi.org/10.1021/ac00083a025.

[16] C. Zhang, B. Gao, L.G. Chen, Q.S. Meng, H. Yang, R. Zhang, X. Tao, H.Y. Gao, Y. Liao, Z.C. Dong, Fabrication of silver tips for scanning tunneling microscope induced luminescence, Rev. Sci. Instrum. 82 (2011) 083101-1-083101–5. https://doi.org/10.1063/1.3617456.

[17] L. Libioulle, Y. Houbion, J.M. Gilles, Very sharp platinum tips for scanning tunneling microscopy, Rev. Sci. Instrum. 66 (1995) 97–100. https://doi.org/10.1063/1.1146153.

[18] S. Kerfriden, A.H. Nahlé, S.A. Campbell, F.C. Walsh, J.R. Smith, The electrochemical etching of tungsten STM tips, Electrochim. Acta. 43 (1998) 1939–1944. https://doi.org/10.1016/S0013-4686(97)00316-2.

[19] M. Lopes, T. Toury, M.L. De La Chapelle, F. Bonaccorso, P. Giuseppe Gucciardi, Fast and reliable fabrication of gold tips with sub-50 nm radius of curvature for tip-enhanced Raman spectroscopy, Rev. Sci. Instrum. 84 (2013) 073702-1-073702–8. https://doi.org/10.1063/1.4812365.

[20] G.N. Meloni, M. Bertotti, 3D printing scanning electron microscopy sample holders: A quick and cost effective alternative for custom holder fabrication,

PLoS One. 12 (2017) 1–12. https://doi.org/10.1371/journal.pone.0182000.

[21] Y. Wen, X. Wang, Characterization and application of a metallic tungsten electrode for potentiometric pH measurements, J. Electroanal. Chem. 714–715 (2014) 45–50. https://doi.org/10.1016/j.jelechem.2013.12.031.

[22] L.M.F. Dantas, P.S. Castro, R.C. Peña, M. Bertotti, Amperometric determination of hydrogen peroxide using a copper microelectrode, Anal. Methods. 6 (2014) 2112–2116. https://doi.org/10.1039/c3ay41980k.

[23] C.G. Zoski, Ultramicroelectrodes : Design , Fabrication , and Characterization, Electroanalysis. 14 (2002) 1041–1051. https://doi.org/https://doi.org/10.1002/1521-4109(200208)14:15/16<1041::AID-ELAN1041>3.0.CO;2-8.

[24] M. Innocenti, C. Zafferoni, A. Lavacchi, L. Becucci, F. Di Benedetto, E. Carretti, F. Vizza, M.L. Foresti, Electroactivation of Microparticles of Silver on Glassy Carbon for Oxygen Reduction and Oxidation Reactions, J. Electrochem. Soc. 161 (2014) D3018–D3024. https://doi.org/10.1149/2.003407jes.

[25] D. Lützenkirchen-Hecht, H.H. Strehblow, Anodic silver (II) oxides investigated by combined electrochemistry, ex situ XPS and in situ X-ray absorption spectroscopy, Surf. Interface Anal. 41 (2009) 820–829. https://doi.org/10.1002/sia.3106.

[26] M. Krebsz, J.P. Kollender, A.W. Hassel, In situ monitoring of the electrochemical dissolution of tungsten, Phys. Status Solidi Appl. Mater. Sci. 214 (2017) 1–5. https://doi.org/10.1002/pssa.201600803.

[27] I.G. Casella, M. Contursi, Electrochemical and spectroscopic characterization of

a tungsten electrode as a sensitive amperometric sensor of small inorganic ions, Electrochim. Acta. 50 (2005) 4146–4154. https://doi.org/10.1016/j.electacta.2005.01.031.

[28] N. Nioradze, R. Chen, J. Kim, M. Shen, P. Santhosh, S. Amemiya, Origins of Nanoscale Damage to Glass-Sealed Platinum Electrodes with Submicrometer Size, Anal. Chem. 85 (2013) 6198–6202. https://doi.org/10.1021/ac401316n.Origins.

[29] V. Eßmann, C. Santana Santos, T. Tarnev, M. Bertotti, W. Schuhmann, Scanning Bipolar Electrochemical Microscopy, Anal. Chem. 90 (2018) 6267–6274. https://doi.org/10.1021/acs.analchem.8b00928.

[30] M.E. Snowden, A.G. Güell, S.C.S. Lai, K. McKelvey, N. Ebejer, M.A. Oconnell, A.W. Colburn, P.R. Unwin, Scanning electrochemical cell microscopy: Theory and experiment for quantitative high resolution spatially-resolved voltammetry and simultaneous ion-conductance measurements, Anal. Chem. 84 (2012) 2483–2491. https://doi.org/10.1021/ac203195h.

[31] V.M. Huang, S.-L. Wu, M.E. Orazem, N. Pébère, B. Tribollet, V. Vivier, Local electrochemical impedance spectroscopy: A review and some recent developments, Electrochim. Acta. 56 (2011) 8048–8057. https://doi.org/10.1016/j.electacta.2011.03.018.

[32] H. Jang, J. Lee, Iridium oxide fabrication and application: A review, J. Energy Chem. 46 (2020) 152–172. https://doi.org/10.1016/j.jechem.2019.10.026.

[33] Z. Zhu, Z. Ye, Q. Zhang, J. Zhang, F. Cao, Novel dual Pt-Pt/IrOx ultramicroelectrode for pH imaging using SECM in both potentiometric and amperometric modes, Electrochem. Commun. 88 (2018) 47–51.

https://doi.org/10.1016/j.elecom.2018.01.018.

[34] L.T. Dimitrakopoulos, T. Dimitrakopoulos, P.W. Alexander, D. Logic, D.B. Hibbert, A tungsten oxide coated wire electrode used as a pH sensor in flow injection potentiometry, Anal. Commun. 35 (1998) 395–398. https://doi.org/10.1039/a807697i.

[35] W. De Zhang, B. Xu, A solid-state pH sensor based on WO3-modified vertically aligned multiwalled carbon nanotubes, Electrochem. Commun. 11 (2009) 1038–1041. https://doi.org/10.1016/j.elecom.2009.03.006.

[36] T.G.S. Babu, T. Ramachandran, B. Nair, Single step modification of copper electrode for the highly sensitive and selective non-enzymatic determination of glucose, Microchim. Acta. 169 (2010) 49–55. https://doi.org/10.1007/s00604-010-0306-4.

[37] A.G. Fogg, S.P. Scullion, T.E. Edmonds, B.J. Birch, Direct reductive amperometric determination of nitrate at a copper electrode formed in situ in a capillary-fill sensor device, Analyst. 116 (1991) 573–579. https://doi.org/10.1039/AN9911600573.

[38] M. Somasundrum, K. Kirtikara, M. Tanticharoen, Amperometric determination of hydrogen peroxide by direct and catalytic reduction at a copper electrode, Anal. Chim. Acta. 319 (1996) 59–70. https://doi.org/10.1016/0003-2670(95)00473-4.

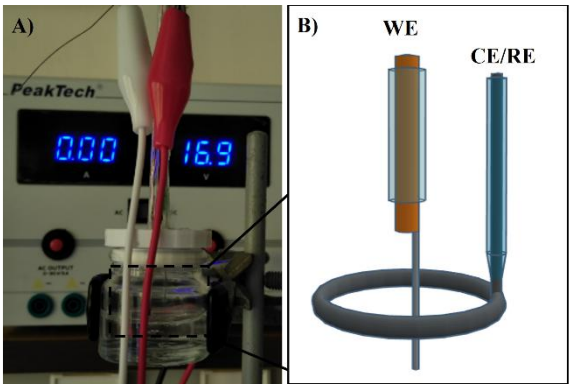

Figure 1. A) Photo of the experimental setup for electrochemical etching of metal wires and carbon fibers. **B)** Scheme of the two-electrode configuration for etching.

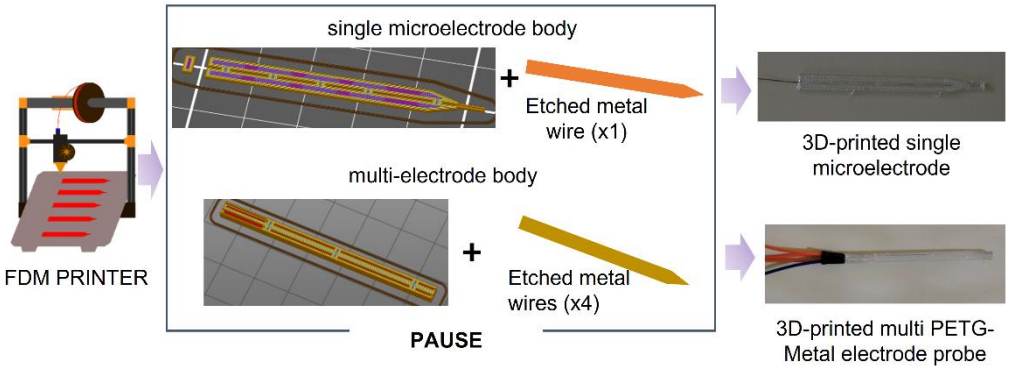

Figure 2. Sequence of fabrication of 3D printed microelectrodes and multi-electrode probe.

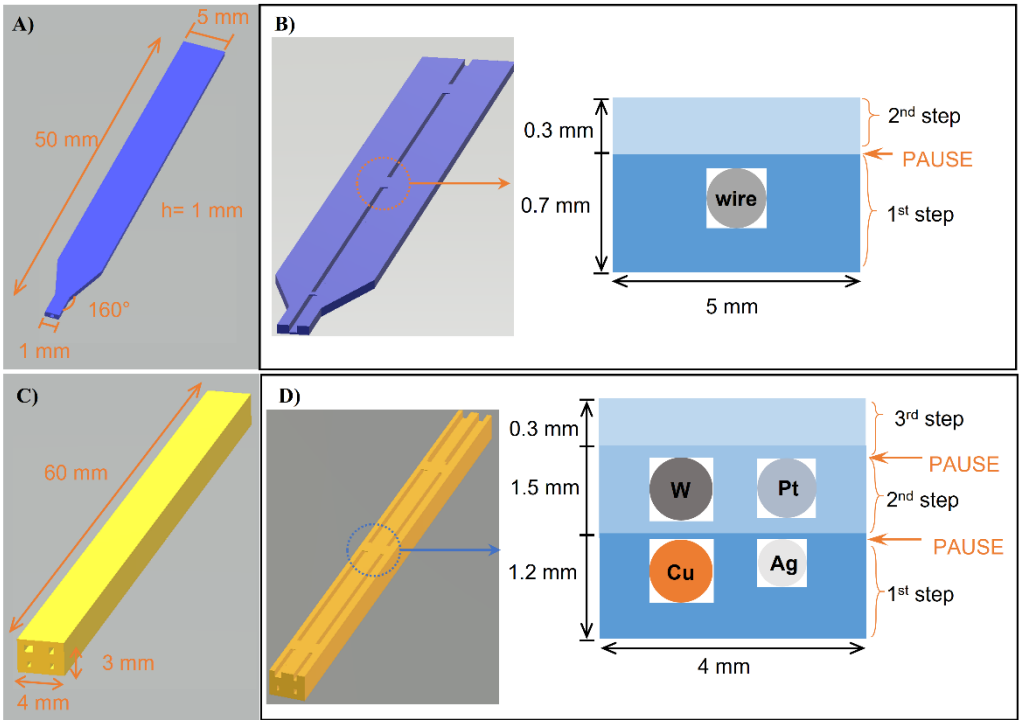

Figure 3. A) Design of a single microelectrode body. **B)** View of the channel at the pause and cross-section view of a "bridge". **C)** Design of a multi-electrode probe body. **D)** View of the channels at the second pause and cross-section view.

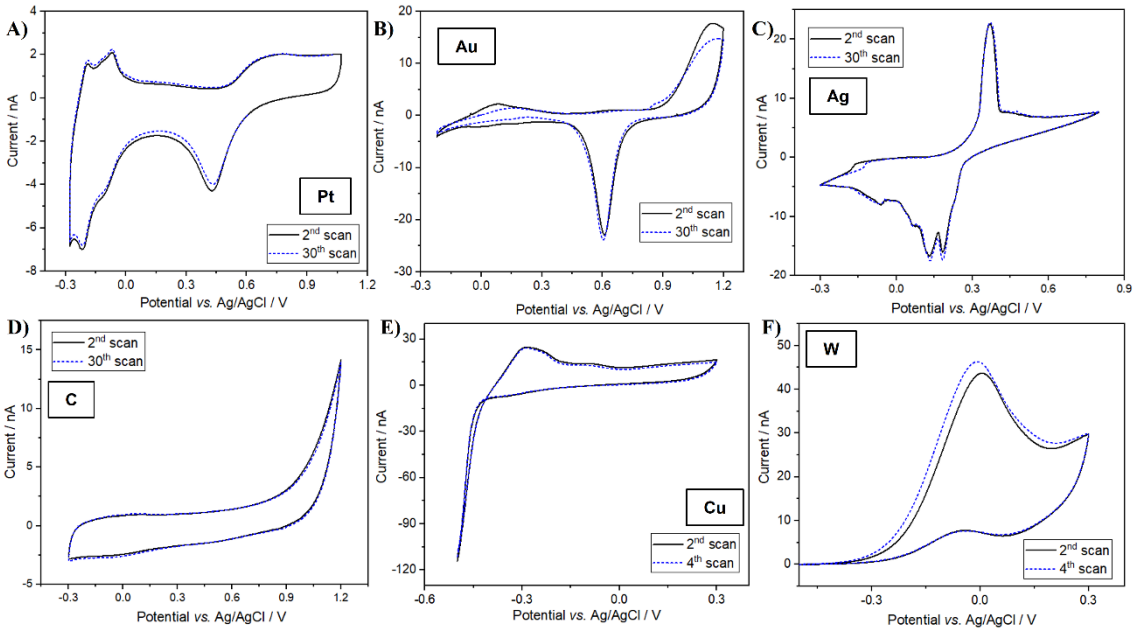

Figure 4. CVs of 3D printed microelectrodes in 0.1 mol/L H_2SO_4 (for Pt, Au, Ag and C) or PBS (pH = 7.4, for Cu and W).

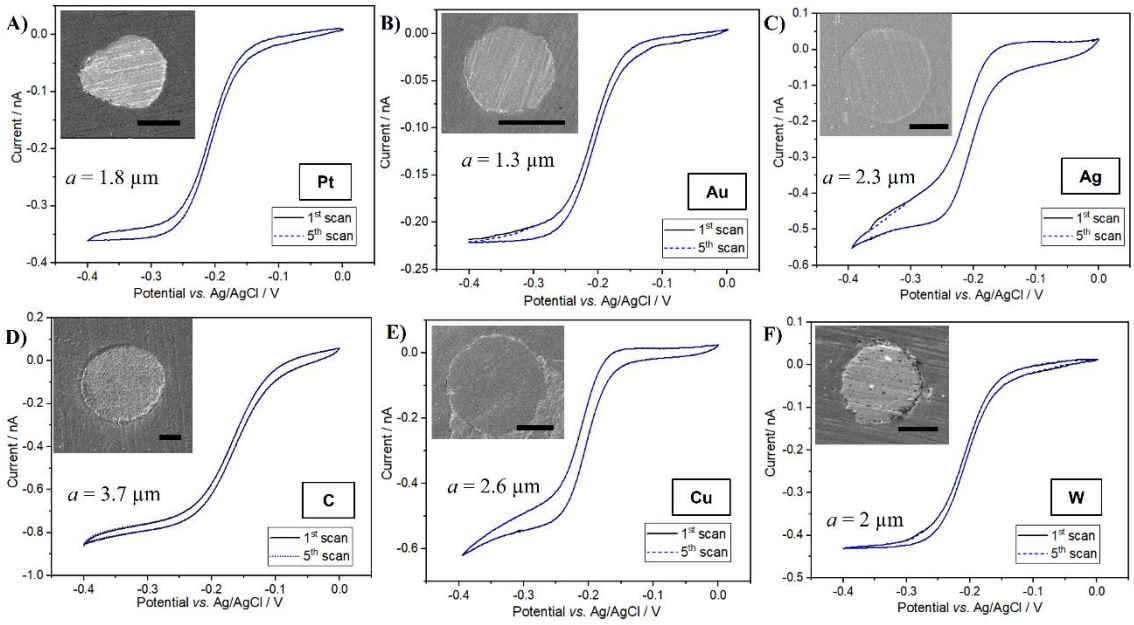

Figure 5. CVs of 3D printed microelectrodes in 1 mmol/L $Ru(NH_3)_6^{3+}$ solution. The inset figures show SEM images of the microelectrodes. Scale bar: 2 µm.

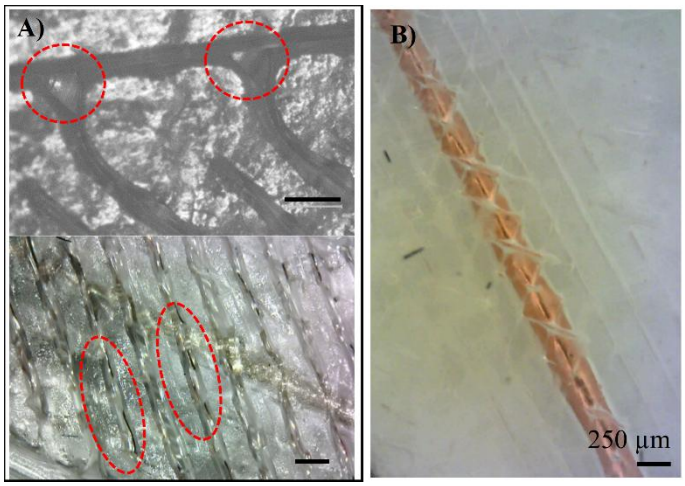

Figure 6. A) Examples of gaps in the as-printed insulating body of microelectrodes. **B)** Photo of the 3D printed microelectrodes after heat post-treatment.

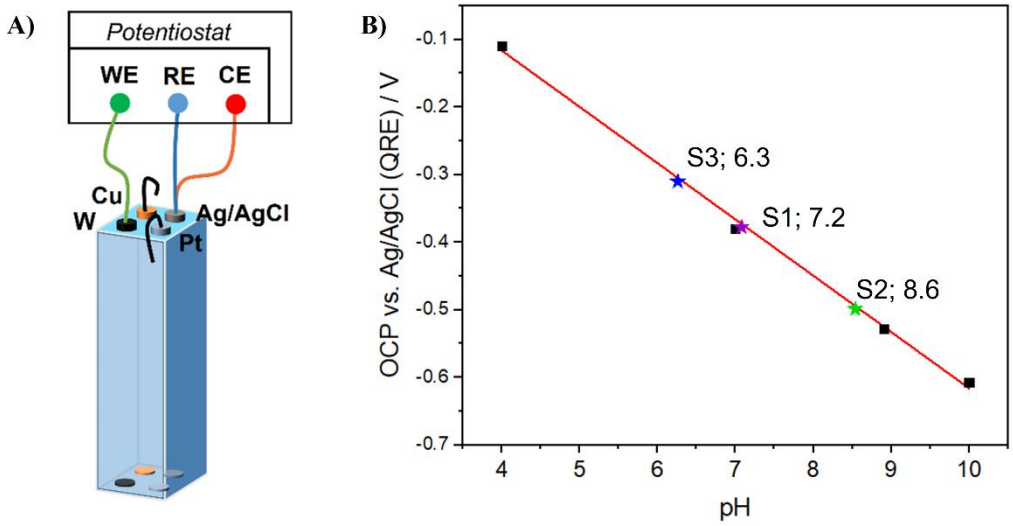

Figure 7. A) Scheme of connection for potentiometric pH determination using a multi-electrode probe. **B)** pH response of the 3D printed multi-electrode probe. (Black squares represent the standard solutions and the red line shows linear regression. Blue, violet and green stars represent samples S3, S1 and S2 respectively).

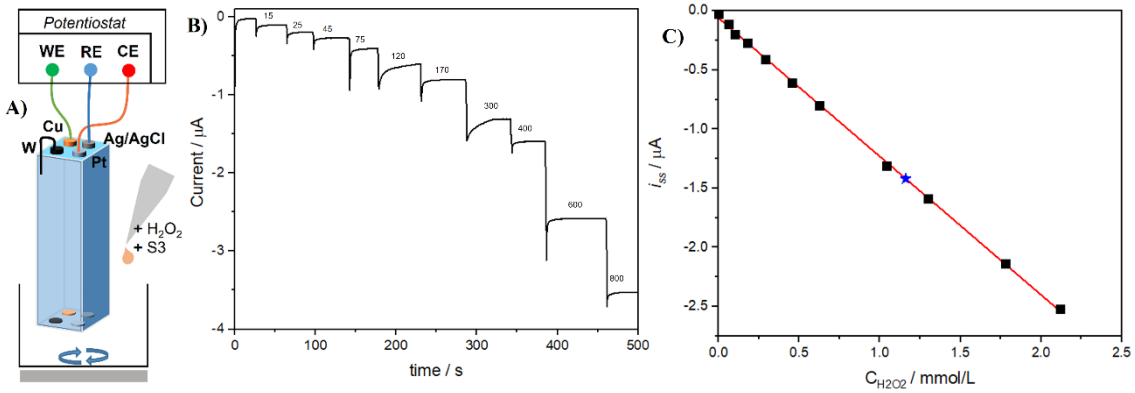

Figure 8. A) Scheme of connection for amperometric determination of H_2O_2 using a multi-electrode probe. **B)** Amperometric response during the calibration of multi-electrode probe. The volume added (µL) is indicated in each step. **C)** Calibration curve of i_{ss} *vs.* C_{H2O2}. (Black squares represent the addition of standard solution and the red lines shows linear regression. The blue star indicates the measure of diluted sample S3).

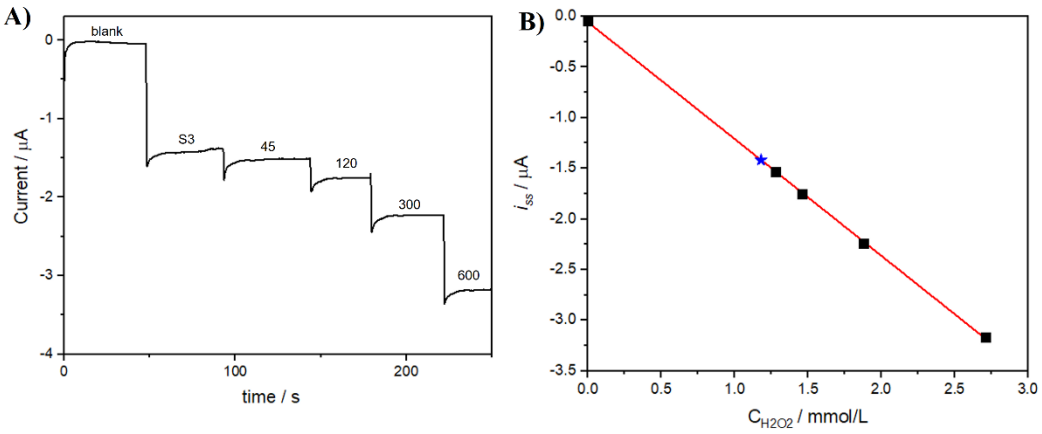

Figure 9. A) Amperometric response during the quantification of sample S3. **B)** Calibration curve of i_{ss} *vs.* C_{H2O2}. (Black squares represent the addition of standard solution and the red line shows linear regression. The blue stars indicates the measure of diluted sample S3).

Credit Author Statement

Mariela Alicia Brites Helú: Methodology, Software, Validation, Formal Analysis, Investigation, Data Curation, Writing-Original Draft, Visualization

Liang Liu: Conceptualization, Resources, Writing-Review & Editing, Funding acquisition